2013 American Control Conference (ACC)
Washington, DC, USA, June 17-19, 2013

An Experimental Comparison of PI, Inversion, and Damping Control for High Performance Nanopositioning

Andrew J. Fleming[1] and Kam K. Leang[2]

Abstract— **This article compares the performance of three feedback control methodologies for high performance nanopositioning applications. Integral resonance damping control is a new approach for controlling mechanical systems. In this approach, the system resonances are actively damped rather than inverted which maximizes the closed-loop bandwidth and provides robustness to changes in the resonance frequencies. This technique is comprehensively compared to the standard methods of PI and inversion control in a practical environment. A five times improvement in the settling-time and bandwidth is demonstrated.**

I. Introduction

High performance nanopositioning stages are required in applications such as: large-range surface inspection [1], [2], scanning probe microscopy [3]–[5], nanofabrication [6]–[9], and imaging of fast biological and physical processes [10]–[13]. To eliminate or reduce the positioning errors arising from resonance excitation, guiding errors, hysteresis, and drift, nanopositioning systems require a feedback and/or feedforward control system.

The most common method for control of nanopositioning system is a combination of PI control and inversion filters [14]. Such techniques can provide excellent closed-loop bandwidth, up to or greater than the resonance frequency [15]. However, to achieve high performance, an extremely accurate system model is required.

Damping control is an alternative method for reducing the bandwidth limitations imposed by mechanical resonance. Damping control uses a feedback loop to artificially increase the damping ratio of a system. An increase in the damping ratio (ζ) allows a proportional increase in the feedback gain and closed-loop bandwidth when using an integral controller. A number of techniques for damping control have been demonstrated successfully in the literature, these include Positive Position Feedback (PPF) [16], polynomial based control [17], shunt control [18]–[20], resonant control [21], Force Feedback [22], [23], and Integral Resonance Control (IRC) [24], [25]. Among these techniques, PPF controllers, velocity feedback controllers, force feedback controllers, and IRC controllers have been shown to guarantee stability when the plant is strictly negative imaginary [26].

Optimal controllers with automatic synthesis have also been successfully applied to nanopositioning applications. Examples include robust $\mathcal{H}_\infty$ controllers [27], [28] and LMI based controllers [29].

This work was supported in part by the Australian Research Council Discovery Project DP120100487.

[1]School of Electrical Engineering and Computer Science, The University of Newcastle, Callaghan, NSW 2308, Australia (andrew.fleming@newcastle.edu.au).

[2]Department of Mechanical Engineering, University of Nevada, Reno, Nevada kam@unr.edu).

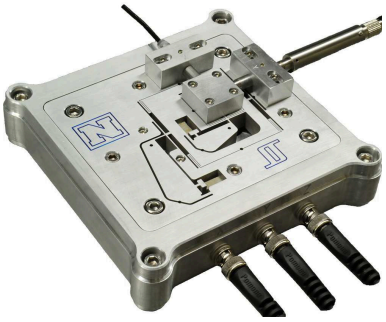

Fig. 1. A two-axis serial-kinematic nanopositioning platform with a range of 30 μm.

Due to their simplicity and robustness, integral resonance controllers have the potential to address the requirements of industrial nanopositioning systems. This article describes the design process for an IRC damping and tracking controller and compares the performance to a PI controller and inverse controller.

II. Experimental Setup

To compare the controller characteristics, each technique will be applied to the two-axis serial-kinematic nanopositioning stage pictured in Figure 1. Each axis contains a 12-mm long piezoelectric stack actuator (Noliac NAC2003-H12) with a free displacement of 12 μm at 200 V. The flexure design includes a mechanical amplifier to provide a total range of 30 μm. The flexures also mitigate cross-coupling so that each axis can be controlled independently. The position of the moving platform is measured by a Microsense 6810 capacitive sensor and 6504-01 probe, which has a sensitivity of 2.5 μm/V. The stage is driven by two PiezoDrive PDL200 voltage amplifiers with a gain of 20.

The x-axis, which translates from left to right in Figure 1, has a resonance frequency of 513 Hz. The y-axis contains less mass so the resonance frequency is higher at 727 Hz. Since the x-axis imposes a greater limitation on performance, the comparison will be performed on this axis. However, the design process for the other axis is identical.

The frequency response for a nominal load is plotted in Figure 2(a). With the maximum payload, the resonance frequency reduces to 415 Hz as shown in Figure 2(b). It can be observed that payload mass significantly modifies the higher frequency dynamics.

For the purpose of control design, a second-order model is procured using the frequency domain least-squares tech-

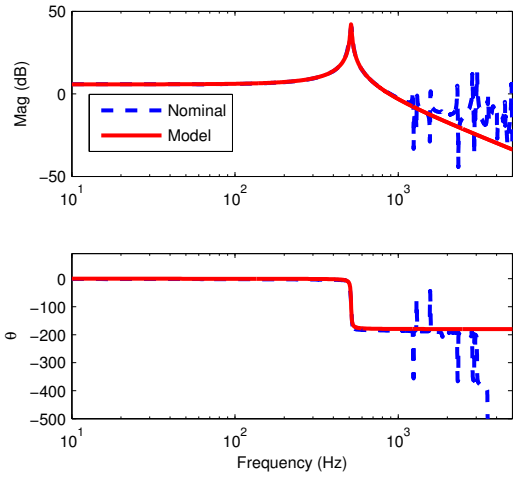

(a) FRF of System and Model

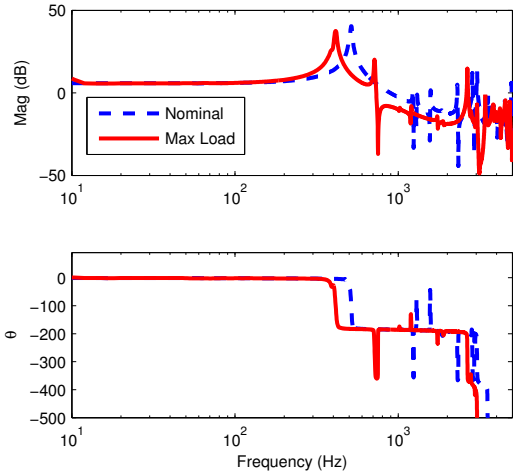

(b) FRF with Nominal and Max Load

Fig. 2. The open-loop frequency response measured from the voltage amplifier input to the sensor output, scaled to μm/V. In (a) the nominal response is compared to the identified model. In (b) the frequency response of the system with maximum load is compared to the nominal response.

niques. The model transfer function is:

$$G(s) = \frac{2.025 \times 10^7}{s^2 + 48.63s + 1.042 \times 10^7}. \quad (1)$$

The frequency response of the model is compared to the experimental data in Figure 2(a). The model closely approximates the first resonance mode which is sufficient for control design.

III. PI Control

A popular technique for control of commercial nanopositioning systems is sensor-based feedback using integral or proportional-integral control [30]. The transfer function of a PID controller is

$$C_{PI}(s) = \beta/s + k_p + k_d s, \quad (2)$$

However, the derivative term is rarely used due to the increased noise sensitivity and stability problems associated

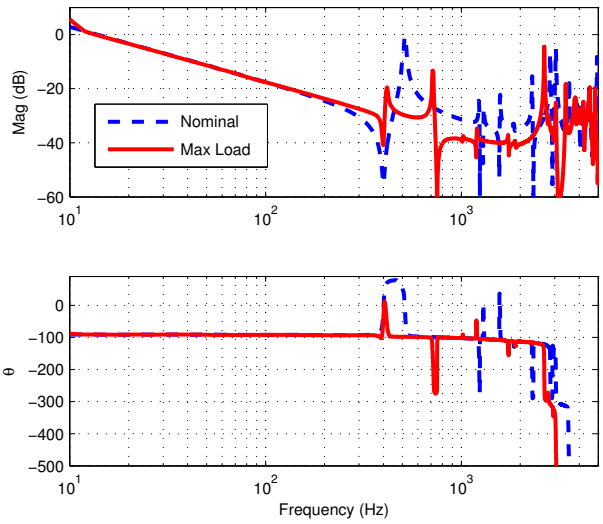

Fig. 3. The loop-gain of the nanopositioner and inversion based controller during nominal and maximum load $C_{Notch}(s)G(s)$.

with high frequency resonance modes. On the other hand, PI controllers are simple to tune and effectively reduce piezoelectric non-linearity at low-frequencies. However, the bandwidth of PI tracking controllers is severely limited by the presence of highly resonant modes. The factor limiting the feedback gain and closed-loop bandwidth is gain-margin [22], [23], [31].

For the nanopositioner under consideration, the maximum permissible gain is 15.5 which is limited by the gain-margin of 6 dB. The closed-loop bandwidth for this controller is only 13 Hz or 2.5% of the resonance frequency. The experimental closed-loop frequency and step responses are plotted in Section VI.

IV. PI Control with Notch Filters

Inversion techniques are popular as they are simple to implement and can provide a high closed-loop bandwidth if they are accurately tuned and the resonance frequency does not vary [14], [15]. The transfer function of a typical inverse controller is

$$C_{Notch}(s) = \frac{\beta}{s} \frac{s^2 + 2\zeta_z s + \omega_w^2}{\omega_z^2} \quad (3)$$

where ζ_z and ω_z are the damping ratio and first resonance frequency of the nanopositioner. Depending on the implementation method, an additional pole may be required above the bandwidth of interest.

A major consideration with inversion based control is the possibility of modeling error. In particular, if the resonance frequency drops below the frequency of the notch filter, the phase lag will cause instability [14]. Therefore, a notch filter must be tuned to the lowest resonance frequency that will occur during service. For example, the example nanopositioner has a nominal resonance frequency of 513 Hz and a minimum resonance frequency 410 Hz. Thus, the notch filter is tuned to 410 Hz with an estimated damping of $\zeta_z = 0.01$.

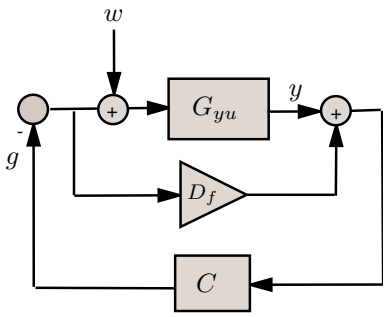

Fig. 4. Integral resonance control scheme [24]

To maintain a gain-margin of 6 dB the maximum integral gain is $\beta = 44$. The loop-gain during nominal and maximum load conditions is plotted in Figure 3. During nominal conditions, the phase-lag does not exceed 180 degrees until the second resonance mode; however, the first resonance mode remains dominant in the response and can be excited by high-frequency components of the input or disturbances. This behavior is evident in the closed-loop frequency and step responses plotted in Section VI. Since the notch filter is tuned to the lowest resonance frequency, the system actually performs better with the maximum payload. The loop-gain in Figure 3 shows that the first resonance-mode is almost inverted during this condition.

Due to the sensitivity of inversion based controllers to variations in the resonance frequency, they are most suited to applications where the resonance frequency is stable, or where the feedback controller can be continually recalibrated [15].

V. Structured PI Control with IRC Damping

Integral Resonance Control (IRC) was first reported as a means for augmenting the structural damping of resonant systems with collocated sensors and actuators [24]. A diagram of an IRC loop is shown in Figure 4. It consists of the collocated system G_{yu}, an artificial feedthrough D_f and a controller C. The input disturbance w represents environmental disturbances.

The first step in designing an IRC controller is to select, and add, an artificial feedthrough term D_f to the original plant G_{yu}. The new system is referred to as $G_{yu} + D_f$. It has been shown that a sufficiently large and negative feedthrough term will introduce a pair of zeros below the first resonance mode and also guarantee zero-pole interlacing for higher frequency modes [24]. Smaller feedthrough terms permit greater maximum damping. Although it is straightforward to manually select a suitable feedthrough term, it can also be computed from Theorem 2 in [24].

For the model G_{yu} described in (1), a feedthrough term of $D_f = -2.5$ is sufficient to introduce a pair of zeros below the first resonance mode. The frequency responses of the open-loop system G_{yu} and the modified transfer function $G_{yu} + D_f$ are plotted in Figure 5.

The key behind Integral Resonance Control is the phase response of $G_{yu} + D_f$, which now lies between -180 and 0

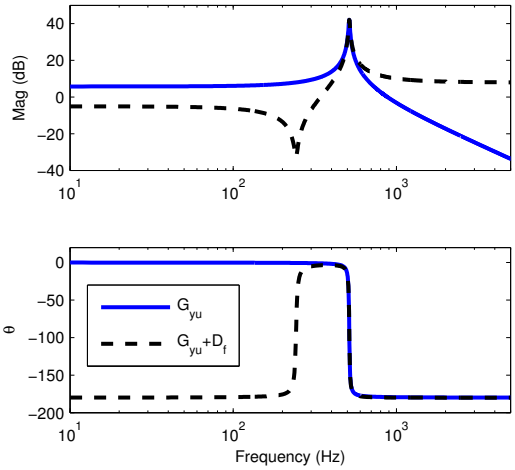

Fig. 5. Frequency response of the open-loop system G_{yu} and with artificial feedthrough $G_{yu} + D_f$, where D_f = -2.5. The 180 degree phase change of $G_{yu} + D_f$ is due to the negative feedthrough which also makes the system inverting.

degrees as shown in Figure 5. Due to the bounded phase of $G_{yu} + D_f$ a simple negative integral controller,

$$C = \frac{-k}{s}, \tag{4}$$

can be applied directly to the system. To examine the stability of such a controller, we consider the loop-gain $C \times (G_{yu} + D_f)$. For stability, the phase of the loop-gain must be within ± 180 degrees while the gain is greater than zero. The phase of the loop-gain $C \times (G_{yu} + D_f)$ is equal to the phase of $G_{yu} + D_f$ minus 180 degrees for the negative controller gain and a further 90 degrees for the single controller pole. The resulting phase response of the loop-gain lies between +90 and -90 degrees. That is, regardless of controller gain, the closed-loop system has a phase margin of 90 degrees and an infinite gain-margin with respect to $G_{yu} + D_f$.

An optimal controller gain k that maximizes damping can be found using the root-locus technique [24]. For the system under consideration, the root-locus in Figure 6 produces a gain of $k = 1900$ and a maximum damping ratio of 0.57.

In order to facilitate a tracking control loop, the feedback diagram must be rearranged in a form where the input does not appear as a disturbance. This can be achieved by finding an equivalent regulator that provides the same loop gain [32]. The equivalent regulator C_2 is [32]

$$C_2 = \frac{C}{1 + CD_f}. \tag{5}$$

When $C = \frac{-k}{s}$ the equivalent regulator is

$$C_2 = \frac{-k}{s - kD_f}. \tag{6}$$

The closed-loop transfer function of the damping loop is,

$$G_{yf} = \frac{G_{yu}C_2}{1 + G_{yu}C_2}. \tag{7}$$

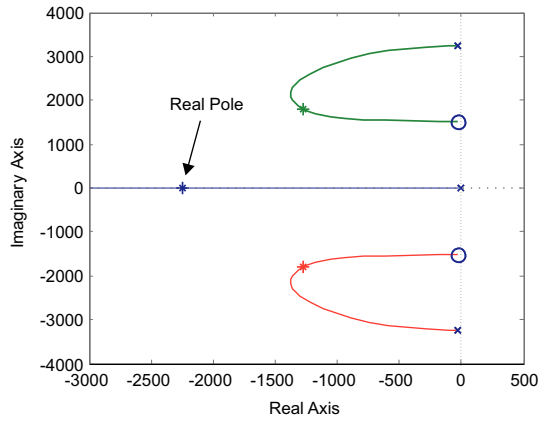

Fig. 6. The root-locus of the damped system G_{yf}. The asterisks mark the optimal pole locations. Note that the closed-loop system contains an additional pole on the real axis.

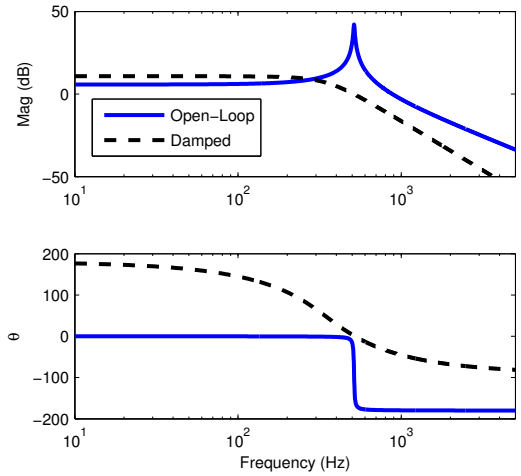

Fig. 7. The open- and closed-loop frequency responses of the system with Integral Resonance control.

With $D_f = -2.5$ and $k = 1900$, the frequency responses of the open-loop and damped systems are plotted in Figure 7.

To achieve integral tracking action, the IRC loop can be enclosed in an outer tracking loop as shown in Figure 8. In previous work, an integral controller has been used for tracking control [32]. However, from the pole-zero map in Figure 6, it can be observed that the damped system contains the resonance poles, plus an additional real axis pole due to the controller. This additional pole unnecessarily increases the system order and reduces the achievable tracking bandwidth. The location of the additional pole can be found by examining the characteristic equation of the damped system, that is

$$1 + G_{yu}C_2 = 0. \tag{8}$$

If G_{yu} has the second-order structure described in equation (1), the characteristic equation can be written

$$\left(s^2 + 2\zeta\omega_n s + w_n^2\right)(s - kD_f) - \omega_n^2 k = 0. \tag{9}$$

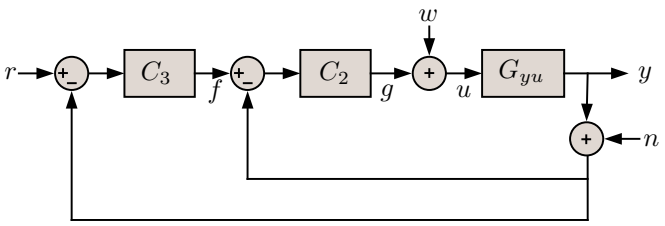

Fig. 8. Tracking control system with the damping controller in regulator form $C_2(s)$ and the tracking controller $C_3(s)$. The signal w is the disturbance input and n is the sensor noise.

For the system under consideration, the roots of equation (9) contain a complex pair and a pole on the real axis. The location of the real pole is most easily found numerically, for example, from the root-locus in Figure 6. In this case, the additional pole is located at $s = -2240$.

To eliminate the additional pole from the tracking loop, the controller can be parameterized so that it contains a zero at the same frequency. A controller that achieves this is

$$C_3 = \frac{-k_i(s + \omega_z)}{s\omega_z}, \tag{10}$$

where ω_z is the frequency of the additional pole identified from equation (9), i.e. $\omega_z = 2240$, and k_i is the integral gain chosen in the normal way to provide the desired stability margins or bandwidth. The form of C_3 is identical to a PI controller except that the zero location is fixed. This is advantageous since the controller has only one free parameter. Note that C_3 is inverting to cancel the inverting nature of G_{yf}.

For the system under comparison, an integral gain of $k_i = 245$ results in a phase margin of 60 degrees. The closed-loop response and performance is examined in Section VI.

The transfer function of the closed-loop system is

$$\frac{y}{r} = \frac{C_3 G_{yf}}{1 + C_3 G_{yf}}, \tag{11}$$

or alternatively,

$$\frac{y}{r} = \frac{C_2 C_3 G_{yu}}{1 + C_2(1 + C_3)G_{yu}}. \tag{12}$$

In addition to the closed-loop response, the transfer function from disturbance to the regulated variable y is also of importance,

$$\frac{y}{w} = \frac{G_{yu}}{1 + C_2(1 + C_3)G_{yu}}. \tag{13}$$

That is, the disturbance input is regulated by the equivalent controller $C_2(1 + C_3)$.

VI. Performance Comparison

In Sections III to V, the controllers were designed to maintain a gain and phase margin of at least 6 dB and 60 degrees. The controller parameters are summarized in Table I and the simulated stability margins are listed in Table II. The integral and inverse controller were limited by gain-margin while the damping controller was limited by phase margin.

PI	$C_3 = \frac{15.5}{s}$
PI + Notch	$C_3 = \frac{44}{s}\,\frac{s^2+50.27s+6.317\times10^6}{6.317\times10^6}\,\frac{2\pi10^3}{s+2\pi10^3}$
PI + IRC	$C_2 = \frac{-245}{s}\,\frac{s+2240}{2240}$, $C_3 = \frac{-1900}{s+4750}$

TABLE I

SUMMARY OF CONTROLLER PARAMETERS

Condition	**PI**	**PI + Notch**	**PI + IRC**
Gain Margin			
Nominal Load	6.1 dB	6.0 dB	14 dB
Full Load	7.0 dB	5.1 dB	10 dB
Phase Margin			
Nominal Load	inf	89°	69°
Full Load	90°	89°	69°
Bandwidth (45°)			
Nominal Load	5.0 Hz	13 Hz	50 Hz
Full Load	5.0 Hz	13 Hz	78 Hz
Settling Time (99%)			
Nominal Load	164 ms	48 ms	9.7 ms
Full Load	165 ms	42 ms	7.6 ms
6σ-Resolution (Peak to Peak Noise)			
Nominal Load	0.27 nm	0.21 nm	0.43 nm

TABLE II

CLOSED-LOOP PERFORMANCE COMPARISON OF THE INTEGRAL, INVERSION, AND DAMPING CONTROLLERS.

The experimental closed-loop frequency responses are plotted in Figure 9. The frequency where the phase-lag of each control loop exceeds 45 degrees is compared in Table II. In nanopositioning applications, the 45 degree bandwidth is more informative than the 3 dB bandwidth since it is more closely related to the settling time. Due to the higher permissible servo gain, the PI+IRC controller provides the highest bandwidth by a significant margin.

The experimental step responses are plotted in Figure 10 and summarized in Table II. The PI+IRC controller provides the shortest step response by approximately a factor of five, however the response exhibits some overshoot.

Out of the three controllers, the combination of PI control and IRC provides the best closed-loop performance under both nominal and full-load conditions. This is the key benefit of damping control, it is more robust to changes in resonance frequency than inverse control. If the variation in resonance frequency were less, or if the resonance frequency was stable, there would not be a significant difference between the dynamic performance of an inverse controller and damping controller. Since the damping controller requires more design effort than an inverse controller, a damping controller is preferable when variance in the resonance frequency is expected, or if there are multiple low-frequency resonances that are difficult to model.

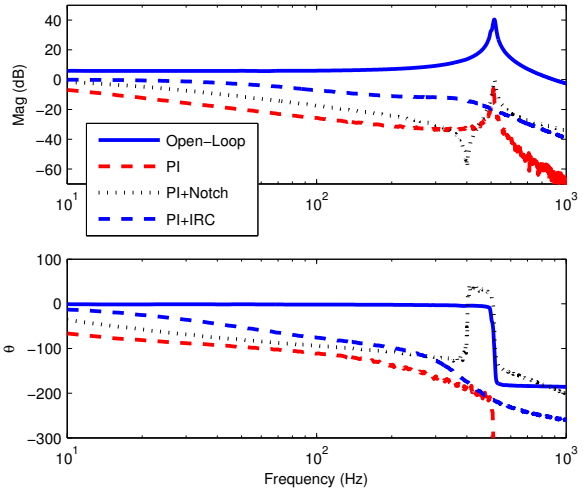

(a) Nominal Load, $f_r = 513$ Hz

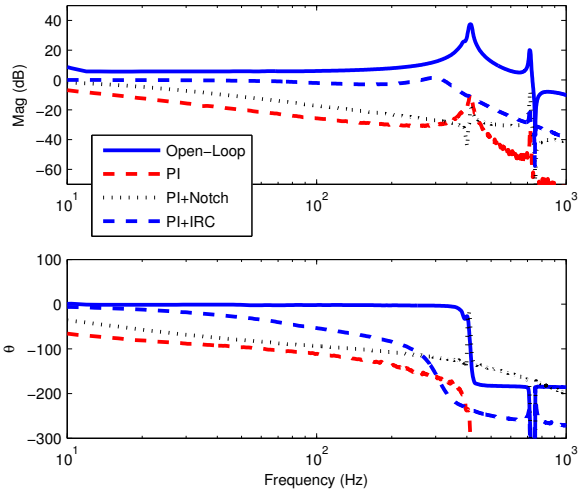

(b) Maximum Load, $f_r = 415$ Hz

Fig. 9. The experimental closed-loop frequency response of each controller under nominal and maximum load conditions.

VII. CONCLUSIONS

This article describes a new method for designing an integral resonance damping controller with integral tracking action. The performance of the new controller is compared to a PI controller and inverse controller which are both common industrial standards.

Although the PI controller was simplest to design and implement, it provided the lowest closed-loop bandwidth. The inverse controller or notch filter can provide much greater bandwidth when the dynamics are well known. However, if the resonance frequency is expected to vary by more than a few percent, the controller must be designed conservatively which limits the achievable performance.

The integral resonance controller damps the system resonance rather than inverting it. The foremost advantages are simplicity, robustness, and insensitivity to variations in the resonance frequencies. In the experimental comparison,

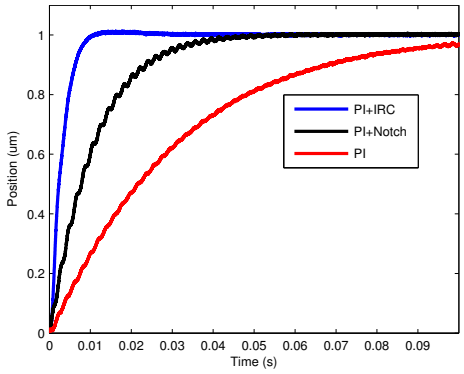

(a) Nominal Load, $f_r = 513$ Hz

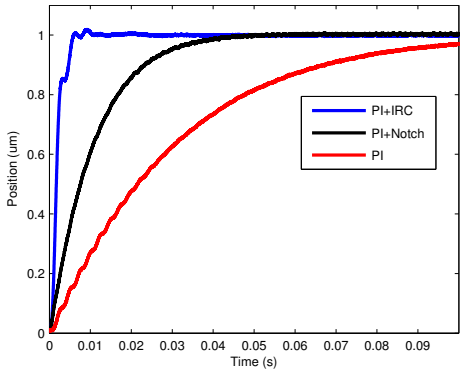

(b) Maximum Load, $f_r = 415$ Hz

Fig. 10. The experimental closed-loop step response of each controller under nominal and maximum load conditions.

where the resonance frequency varied by 19%, the settling-time of the IRC controller with one-fifth that of the inverse controller.

REFERENCES

[1] G. Borionetti, A. Bazzalia, and R. Orizio, "Atomic force microscopy: a powerful tool for surface defect and morphology inspection in semiconductor industry," *The European Physical Journal Applied Physics*, vol. 27, no. 1-3, pp. 101–106, July 2004.

[2] A. Humphris, M. McConnell, and D. Catto, "A high-speed atomic force microscope capable of video-rate imaging," *Microscopy and Analysis - SPM Supplement*, pp. 29–31, March 2006.

[3] M. J. Brukman and D. A. Bonnell, "Probing physical properties at the nanoscale," *Physics Today*, vol. 61, no. 6, pp. 36–42, June 2008.

[4] Y. F. Dufrêne, "Towards nanomicrobiology using atomic force microscopy," *Nature Reviews Microbiology*, vol. 6, pp. 674–680, September 2008.

[5] N. Jalili and K. Laxminarayana, "A review of atomic force microscopy imaging systems: application to molecular metrology and biological sciences," *Mechatronics*, vol. 14, no. 8, pp. 907–945, October 2004.

[6] A. Ferreira and C. Mavroidis, "Virtual reality and haptics for nanorobotics," *IEEE Robotics and Automation Magazine*, vol. 13, no. 3, pp. 78–92, September 2006.

[7] A. A. Tseng, S. Jou, A. Notargiacomo, and T. P. Chen, "Recent developments in tip-based nanofabrication and its roadmap," *Journal of Nanoscience and Nanotechnology*, vol. 8, no. 5, pp. 2167–2186, May 2008.

[8] A. A. Tseng, Ed., *Nanofabrication: Fundamentals and Applications*. Singapore: World Scientific, 2008.

[9] J. A. Vicary and M. J. Miles, "Pushing the boundaries of local oxidation nanolithography: Short timescales and high speeds," *Ultramicroscopy*, vol. 108, no. 10, pp. 1120–1123, September 2008.

[10] G. Schitter, R. W. Stark, and A. Stemmer, "Fast contact-mode atomic force microscopy on biological specimens by model-based control," *Ultramicroscopy*, vol. 100, pp. 253–257, 2004.

[11] T. Ando, N. Kodera, T. Uchihashi, A. Miyagi, R. Nakakita, H. Yamashita, and K. Matada, "High-speed atomic force microscopy for capturing dynamic behavior of protein molecules at work," *e-Journal of Surface Science and Nanotechnology*, vol. 3, pp. 384–392, December 2005.

[12] G. E. Fantner, G. Schitter, J. H. Kindt, T. Ivanov, K. Ivanova, R. Patel, N. Holten-Andersen, J. Adams, P. J. Thurner, I. W. Rangelow, and P. K. Hansma, "Components for high speed atomic force microscopy," *Ultramicroscopy*, vol. 106, no. 2-3, pp. 881–887, June-July 2006.

[13] M. Kobayashi, K. Sumitomo, and K. Torimitsu, "Real-time imaging of DNAstreptavidin complex formation in solution using a high-speed atomic force microscope," *Ultramicroscopy*, vol. 107, no. 2-3, pp. 184–190, February-March 2007.

[14] K. K. Leang and S. Devasia, "Feedback-linearized inverse feedforward for creep, hysteresis, and vibration compensation in AFM piezoactuators," *IEEE Transactions on Control Systems Technology*, vol. 15, no. 5, pp. 927–935, September 2007.

[15] D. Y. Abramovitch, S. Hoen, and R. Workman, "Semi-automatic tuning of PID gains for atomic force microscopes," in *Proc. American Control Conference*, Seattle, WA, June 2008, pp. 2684–2689.

[16] J. L. Fanson and T. K. Caughey, "Positive position feedback control for large space structures," *AIAA Journal*, vol. 28, no. 4, pp. 717–724, 1990.

[17] S. S. Aphale, B. Bhikkaji, and S. O. R. Moheimani, "Minimizing scanning errors in piezoelectric stack-actuated nanopositioning platforms," *IEEE Transactions on Nanotechnology*, vol. 7, no. 1, pp. 79–90, January 2008.

[18] A. J. Fleming and S. O. R. Moheimani, "Sensorless vibration suppression and scan compensation for piezoelectric tube nanopositioners," *IEEE Transactions on Control Systems Technology*, vol. 14, no. 1, pp. 33–44, January 2006.

[19] ——, "Control oriented synthesis of high performance piezoelectric shunt impedances for structural vibration control," *IEEE Transactions on Control Systems Technology*, vol. 13, no. 1, pp. 98–112, January 2005.

[20] S. S. Aphale, A. J. Fleming, and S. O. R. Moheimani, "High speed nano-scale positioning using a piezoelectric tube actuator with active shunt control," *IET Micro & Nano Letters*, vol. 2, no. 1, pp. 9–12, March 2007.

[21] A. Sebastian, A. Pantazi, S. O. R. Moheimani, H. Pozidis, and E. Eleftheriou, "A self servo writing scheme for a MEMS storage device with sub-nanometer precision," in *Proc. IFAC World Congress*, Seoul, Korea, July 2008, pp. 9241–9247.

[22] A. J. Fleming, "Nanopositioning system with force feedback for high-performance tracking and vibration control," *IEEE Transactions on Mechatronics*, vol. 15, no. 3, pp. 433–447, June 2010.

[23] A. J. Fleming and K. K. Leang, "Integrated strain and force feedback for high performance control of piezoelectric actuators," *Sensors and Actuators A*, vol. 161, no. 1-2, pp. 256–265, June 2010.

[24] S. S. Aphale, A. J. Fleming, and S. O. R. Moheimani, "Integral resonant control of collocated smart structures," *IOP Smart materials and Structures*, vol. 16, pp. 439–446, April 2007.

[25] B. Bhikkaji and S. O. R. Moheimani, "Integral resonant control of a piezoelectric tube actuator for fast nanoscale positioning," *IEEE/ASME Transactions on Mechatronics*, vol. 13, no. 5, pp. 530–537, October 2008.

[26] I. Petersen and A. Lanzon, "Feedback control of negative-imaginary systems," *Control Systems, IEEE*, vol. 30, no. 5, pp. 54 –72, oct. 2010.

[27] S. Salapaka, A. Sebastian, J. P. Cleveland, and M. V. Salapaka, "High bandwidth nano-positioner: A robust control approach," *Review of Scientific Instruments*, vol. 75, no. 9, pp. 3232–3241, September 2002.

[28] A. Sebastian and S. Salapaka, "Design methodologies for robust nano-positioning," *IEEE Transactions on Control Systems Technology*, vol. 13, no. 6, pp. 868–876, November 2005.

[29] C. Lee and S. Salapaka, "Fast robust nanopositioning: A linear-matrix-inequalities-based optimal control approach," *IEEE/ASME Transactions on Mechatronics*, vol. 14, no. 4, pp. 414–422, August 2009.

[30] Y. Li, K. H. Ang, and G. Chong, "PID control system analysis and design," *Control Systems, IEEE*, vol. 26, no. 1, pp. 32–41, February 2006.

[31] A. J. Fleming, "Dual-stage vertical feedback for high speed-scanning probe microscopy," *IEEE Transactions on Control Systems Technology*, vol. 19, no. 1, pp. 156–165, January 2011.

[32] A. J. Fleming, S. S. Aphale, and S. O. R. Moheimani, "A new method for robust damping and tracking control of scanning probe microscope positioning stages," *IEEE Transactions on Nanotechnology*, vol. 9, no. 4, pp. 438–448, September 2010.